**Article:**
Hodgkinson, R., Brambila, C., Nutter, J. et al. (1 more author) (2025) Rapid, in-line characterisation of a vortex mixer and its use for green synthesis of nanosilica. Chemical Engineering and Processing - Process Intensification. 110578. ISSN: 0255-2701

https://doi.org/10.1016/j.cep.2025.110578

# Rapid, in-line characterisation of a vortex mixer and its use for green synthesis of nanosilica

*Richard Hodgkinson[#], Carlos Brambila[#], John Nutter, Siddharth Patwardhan**

*School of Chemical, Materials and Biological Engineering,*
*The University of Sheffield, Mappin Street, Sheffield, S1 3JD, UK*
*[#] These authors contributed equally.*
** Corresponding author: s.patwardhan@sheffield.ac.uk*

# Abstract

Scaling-up nanomaterials synthesis is complex due to a lack of understanding of the effects of mixing and production scales on the process chemistry. Use of intensified mixer provides a way forward to address these challenges. To that end, this study represents a first step towards exploring the use of a vortex mixer to study the effects of mixing on the formation of nanosilica using a bioinspired green synthesis. Firstly, we designed a multi-inlet vortex mixer (MIVM) and characterised its mixing profile. To facilitate this process, enable faster measurements and address variability in the results, we designed and implemented an in-line measurement setup. The in-line setup was then used to characterise a vortex mixer and the results show excellent match between the custom-built setup and the traditional offline method, thus demonstrating its ability to provide a rapid and simple way for quantifying mixing. Finally, we explored the implementation of a MIVM for the green synthesis of silica for the first time. We observed that at higher flowrates when MIVM provides fast mixing, the conversion of the precursor, the yield and the product properties approached those of silica obtained from an ideally mixed batch system. Collectively, these results provide a clear pathway to help design future investigations to correlate the mixing conditions with emerging nanomaterials syntheses as well as enable their scale-up by implementing adequate mixing processes.

# Introduction

Nanomaterials have wide ranging applications in medicine, environmental engineering, energy sector and beyond due to their unique properties when compared to bulk materials.[1] However, despite many nanomaterials being discovered, very few materials such as silica, zinc oxide and titania have reached the market due to a lack of sustainable and scalable synthesis methods for producing high-value products. Often, their scale-up is challenging and the underpinning science of scale-up is unknown. For example, without understanding the changes in mixing with scale and their consequent impact of nanomaterials formation and properties, larger scale syntheses lead to undesirable products.

One such example is silica – while low-value silica (precipitated and gel) is manufactured commercially, high-value silica such as mesoporous silicas (MCM-41 or SBA-15) are uneconomical and unsustainable to manufacture at scale.[2, 3] To overcome these issues, learning from biology and incorporating green chemistry principles, a new class of bioinspired silicas (BIS) have been discovered. Bioinspired silica has shown significant advantages over traditional silica synthesis methods,[4] in producing functional nanomaterials in a more sustainable,[2] efficient, and scalable way,[5] which can transform industries that rely on silica-based materials.[1] Bioinspired synthesis offers control over a range of critical quality attributes and this flexibility allows for the design for products for use in catalysis, drug delivery, sensors, and coatings, among other applications.[5] Despite progress made on BIS synthesis, research on its scale-up and process intensification has only begun recently.[6, 7]

Mixing, which changes with scale-up, influences the distribution of precursor materials with reactant heterogeneities thus affecting reaction kinetics and pathways, which impacts final nanomaterial characteristics such as particle size, size distribution, morphology and porosity.[6] Nanomaterials syntheses, such as traditional silica formation, exhibit complexity in scale-up due to numerous steps involved in their formation such as nucleation, polymerisation, growth and precipitation/crystallisation.[8] Bioinspired silica (BIS) synthesis,

which follows non-classical formation pathways and involves additional steps such as pre-nucleation, clustering, and self-assembly.[5] For example, Schaer *et. al* showed that mixing influenced the conversion of silicate monomers to oligomers and particles during silica synthesis with impacts on porosity and particle size.[9] Research has also demonstrated that in conventional synthesis of silica nanoparticles, using microreactors or micromixers can produce narrower particle size distributions and higher reactant conversions compared to traditional batch reactors.[10] Similarly, mixing in continuously stirred tank reactors (CSTRs) has been shown to affect the aggregation and growth of nanoparticles in general.[11]

We recently studied mixing effects on BIS synthesis using a CSTR and found that certain reaction steps in BIS formation were sensitive to mixing, with variations in impeller speed and feed location influencing particle size and pore structure.[6] While CSTRs are easy to use for such mixing studies, they have a wide distribution of mixing/residence times, and investigating effects of a wider range of mixing scenarios (e.g. higher energy dissipation representing pilot- or larger-scales) becomes practically challenging. To this end, continuous in-line mixers such as the continuous impinging jet (CIJ) and multi inlet vortex mixer (MIVM), along with similar geometries such as the Roughton mixer, allow practical mapping of a wide range of mixing conditions, yet at a smaller footprint compared to CSTRs, and have been applied to a range of applications.[8, 12-23] Further, given the rapid nature of BIS synthesis (seconds to minutes), unlike conventional syntheses, in-line mixers provide a way for developing continuous synthesis that is suitable for Plug Flow Reactors (PFRs) at commercial scales.

With this background on the green synthesis of nanomaterials and challenges in their scale-up, this study represents a first step towards exploring the use of in-line mixers to study the effects of wider mixing intensities on BIS formation. As such, there are two aims as described below. Firstly, we aim to design an MIVM and characterise its mixing profile using a custom-built in-line measurement system. MIVM are preferred here since they can operate with unequal stream flowrates vs. CIJ mixers,[12-15] an additional controllable factor for our

chemically distinct inlets. There are a number of routes to experimentally characterise mixing timescales,[24] here we use the well-known Villermaux-Dushman competing chemical reaction system (VD reactions). To facilitate this process and look to eliminate sources of variability in initial manually sampled data obtained, we design and implement an in-line optical absorbance setup operating at an alternate, easier to achieve wavelength. In-line measurements have been reported in the literature typically using commercial equipment and occasionally utilising alternate wavelengths,[25-29] but for our study we instead designed and constructed a simple, low cost VD-specific automated in-line absorbance measurement, described herein. Secondly, our aim is to the explore the implementation of a MIVM for BIS synthesis for the first time to investigate the impact of mixing timescales on critical quality attributes, benchmarking the resulting materials against a conventional small-scale batch reaction. This will help design future investigations to correlate the associated mixing conditions and timescales with the product properties obtained as well as better understand the practicalities of implementing continuous mixing processes.

# Experimental Methods

### MIVM design and pumping system

For both the silica synthesis and Villermaux-Dushman mixing characterisation in this work, the MVIM shown in Figure 1 was used, 3D printed from polymer resin. The mixer has two tangential inlet ports (one with a retrofitted tangential pressure tap, plugged for this work) and short axial outlet port. Flow was provided from two World Precision Instruments AL-1050 syringe pumps, typical in many laboratories, fitted with 100ml Samco ground glass syringes. Silicone tubing was used for interconnections, ~3mm in diameter. Although this pumping set-up is commonly used in various labs, small fluctuations in flows were observed, (see Supporting Information) hence, we reported average absorbance values over an integer number of oscillation cycles. Outflow either proceeds via a short length of tubing, to the in-line optical absorption cell in the case of VD characterisation, or into a final container in the

case of silica synthesis. Flowrates of 6, 12, 20, 30, and 42 ml/min per pump were used, with the mixing conditions assumed identical given that all aqueous solutions used were dilute with limited viscosity differences.

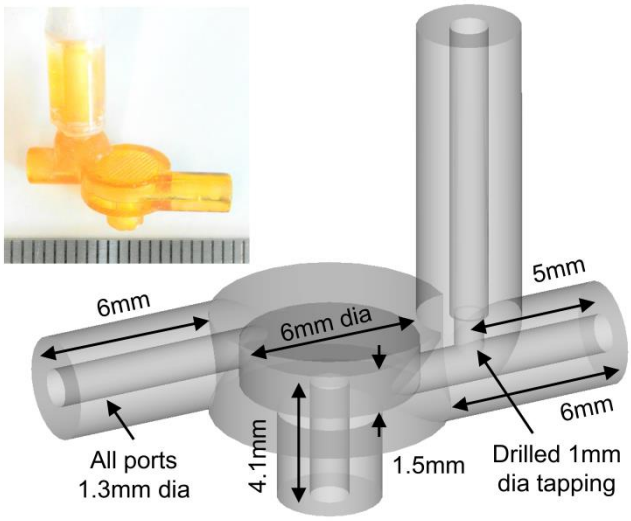


Figure 1: Design and photograph (inset) of MIVM (ruler increments in photo are in mm).

## Custom-made in-line optical measurements for mixing characterisation

Briefly, the Villermaux-Dushman protocol consists of two reactions competing for $H^+$ – an almost instantaneous neutralisation to form hydroboric acid (Equation 1) and a modestly fast reaction between iodide ($I^-$) and iodate ($IO_3^-$) ions to form iodine (Equation 2).[24, 30, 31] The iodine formed can then react with iodide to form triiodide ($I_3^-$) via Equation 3, which is readily quantifiable by optical absorbance. On occurrence of slow mixing, local regions of excess proton concentration result in the neutralisation reaction going to completion and the redox reaction forming coloured triiodide ions. This was then converted to an estimate of mixing timescales through relations based on reaction kinetics and a predetermined mixing model following literature protocols.[24]

$$H_2BO_3^- + H^+ \rightarrow H_3BO_3 \quad \text{... Equation 1}$$

$$5I^- + IO_3^- + 6H^+ \rightarrow 3I_2 + 3H_2O \quad \text{... Equation 2}$$

$$I_2 + I^- \leftrightarrow I_3^- \quad \text{... Equation 3}$$

The triiodide product is typically measured manually, with samples being loaded in a conventional UV-VIS spectrophotometer for absorption measurement at 353 nm. However, this is tedious, especially with multiple flowrates/geometries. For a custom apparatus measuring at 353 nm needs special photosensors, UV LEDs and focussing optics, however, the triiodide product has appreciable absorption at 405 nm[32], permitting inexpensive pre-focused LEDs and sensors. Pairing such an LED (VAOL-5EUV0T4, 15° beam, 200 mcd, VCC) and a large area photodiode (BPW21, 7.34 $mm^2$, Osram) permitted useful sensitivity.

Shown in Figure 2 is the 3D printed in-line optical absorbance unit and associated flow cell. This first iteration setup (see Supporting Information for remarks) has been designed considering the requirements in the literature for continued mixing to completion[24, 33] and to address potential coating of the flow-through cell walls.[24] A polystyrene tapered disposable cuvette (Fisherbrand FB55147) of 10 mm optical path length was used, onto which a single 3D printed outlet port was glued. A 3D printed insert with two inlet ports minimised dead space, and a micro stir bar (8x3mm bar, Fisherbrand 11818892) completes mixing vs. the standard literature practice of long outlet pipe runs. This cell inserts into an optical well in the 3D printed housing, featuring a magnetically coupled DC motor stir bar drive, a solenoid shutter for automated dark level calibration (avoids disturbing the source LED), and a peristaltic pump for bright level calibration via water flushing. In operation this was used inverted, with the cell outlet port uppermost for purging bubbles from the system via an initial fast water/reagent flush and rapid stir bar rotation. The LED was provided with 20.7 mA from a constant current source, and a time-filtered transimpedance amplifier (constructed around an LM358 op-amp) interfaced to a Digilent AD2 USB oscilloscope for data capture. Open beam photodiode photocurrent was about 15 µA. The AD2 also powered the setup (optical section via separate regulators), controlled the shutter stirrer and pump, as well as interfaced to a pressure sensor to permit initial choice of a reaction set from $t_{mix}$ estimates using the pressure drop (as suggested in ref.[24]). A warm-up period was provided to allow the

electronics to fully stabilise. The overall setup, as well as the syringe pumps used, was operated automatically from a custom program written in LabVIEW.

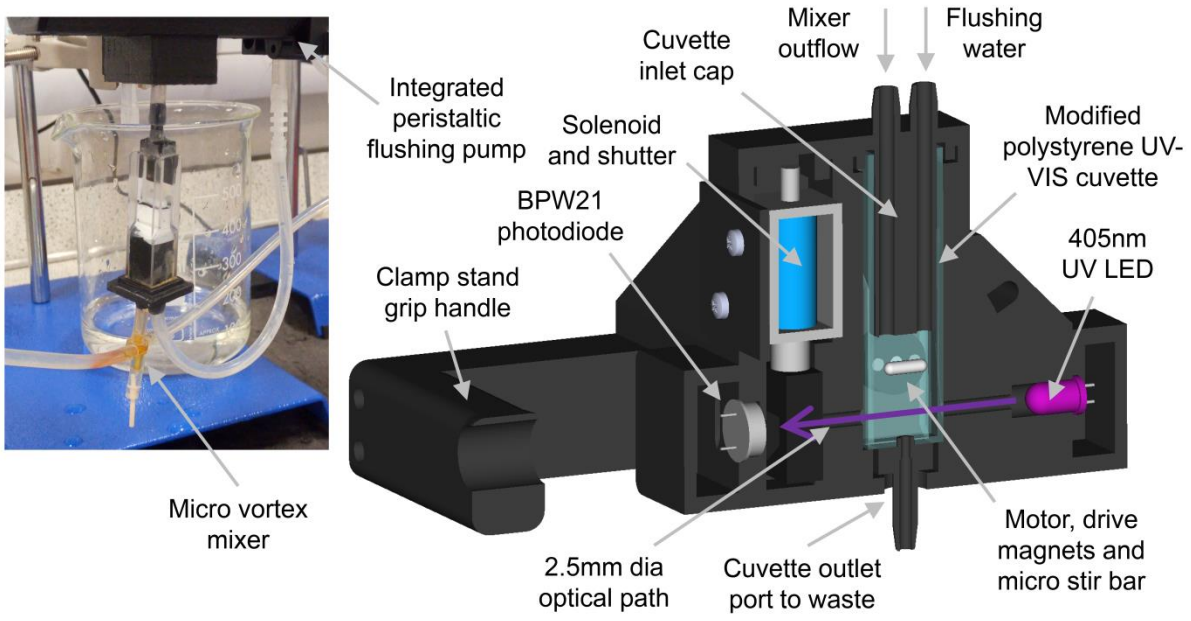


Figure 2: Design of custom-built in-line Villermaux-Dushman measurement setup and photograph (inset) of modified polystyrene cuvette in use.

## Villermaux-Dushman (VD) reactions

For the VD measurements performed in this work, concentration set 1C of ref.[24] (known to be suitable from initial manual work) was used to prepare the sulphuric acid and buffer solutions and addition sequence precautions of ref.[34] were followed. Due to the impracticality of preparing all reagents immediately before use, we prepared stock solutions of KI, $KIO_3$, NaOH, $H_3BO_3$ and $H_2SO_4$ aqueous solutions using nitrogen bubbled water (<0.4mg/L $O_2$ concentration) and kept them sealed (and in dark, for iodine species) before use. Since solution makeup increased $O_2$ levels to around 2mg/L, aliquots of these were then separately bubbled with nitrogen to <0.4mg/L $O_2$ before being gently combined immediately prior to an experimental run. For all experiments, pH values of prepared buffer ranged from $10.92 \pm 0.25$ and of mixed solutions from $9.65 \pm 0.15$, satisfying expected values and constraints in literature.[24, 34] Data from the in-line setup (405nm, 10mm path length) was adjusted later for the 353nm, 5mm path length of literature $t_{mix}$ correlations.[24] The reduced

absorbance through operating at 405nm vs. 353nm, shown later, actually improves overall system sensitivity: photocurrent is already small, proportional to and digitised in terms of transmission %, meaning it should be optimised to be between e.g. 20-100%, vs. the published 353nm (5mm) $t_{mix}$ relations covering ~70% to <<1%. The Supporting Information describes how in-line measurements were ran, presents an exemplar absorbance data time series, and describes subsequent data processing to produce the result.

## Bioinspired Silica Synthesis

Sodium silicate pentahydrate (Fisher Scientific, technical grade) and tetraethylenepentamine (TEPA, Sigma-Aldrich, technical grade) were used as received. HCl (37.0 wt %, Honeywell Fluka) was diluted with deionized water (Millipore, >16 MΩ·cm) as required.

Bioinspired silica synthesis was performed as described elsewhere[35] and the reaction scheme can be simplified as shown in Equation 4. Briefly, two stock solutions were prepared: solution A consisted of sodium silicate (30 mmol) combined with approximately 6.5 mL of 1M HCl and diluted to 500 mL with deionised water. Separately, solution B consisted of TEPA (6 mmol) diluted to 500 mL with deionised water. These solutions were used for both the batch and MIVM mixing processes. Preliminary experiments were performed to determine the amount of acid needed to achieve pH 7 in the mixing step. This was achieved via fine tuning syringe flowrates in the MIVM synthesis (final pH was 7.00±0.08) or addition of drops of acid during the first 5 seconds during batch mixing synthesis (final pH was 7.00±0.2).

$$\text{Silicic acid monomer } [Si(OH)_4] \rightarrow \text{silicate oligomers} \rightarrow \text{silica product } [SiO_2] \quad \textbf{...Equation 4}$$

For continuous silica synthesis with the MIVM, synthesis was conducted at the same flowrate series and with the same pump/mixer setup as previously described with the MIVM outflow proceeding through a short tube (6 cm long 3 mm diameter) into a gently stirred plastic tub (20 mm stir bar, 50 mm diameter beaker, ~300 rpm without forming a vortex). For the batch mix experiments, 50 ml of solution A and B were rapidly added to a vigorously

stirred plastic tub of the same diameter above and allowed to react for 5 minutes under stirring. This provided an ideally mixed benchmark for comparison.

In all cases, solutions were subsequently left to stand after mixing (either via the MIVM or in a tub) so that all reactions lasted for ~20 minutes (see Figure 3) before the solid bioinspired silica coagulum was isolated by centrifugation at 5000g for 7 minutes and the supernatant retained for subsequent silica speciation and yield analysis. The solid pellet was resuspended in 50 mL of deionized water and centrifuged again; this process was repeated twice. The resulting material was dried overnight at 40 °C. All silica synthesis experiments for both MIVM and batch were performed at least three times.

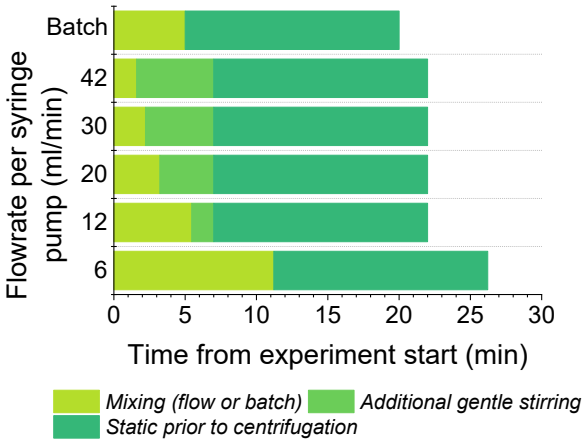


Figure 3: Graphical summary of timescale of reaction steps used with MIVM and batch mixing experiments.

## Gas Adsorption for Porosity Analysis

Nitrogen adsorption isotherms at 77 K were obtained using a Micromeritics Tristar adsorption analyser. Approximately 50 mg of each sample was weighed into a sample tube, which was then degassed at 120 °C using a vacuum heating manifold. After at least 4 hours of degassing, samples were reweighed and placed in the Tristar for analysis. Isotherms were analysed using Micromeritics MicroActive software to calculate Brunauer-Emmett-Teller (BET) surface areas, and Barrett-Joyner-Halenda (BJH) desorption models were applied to determine pore size distributions.

## Silica Speciation and Yield Analysis

Silica speciation and the extent of the reaction were determined using the silicomolybdate blue spectrophotometric method.[36] A molybdic acid solution was prepared by dissolving ammonium molybdate tetrahydrate (51 mmol) in 60 mL of 37 wt % HCl solution and 500 mL of water, followed by dilution with deionized water to a final volume of 1 L. A reducing agent solution was prepared by dissolving oxalic acid (111 mmol), anhydrous sodium sulphite (2 g), and N-methyl-p-aminophenol hemisulphate (10 mmol) in 250 mL of deionized water, followed by dilution to 500 mL.

For the analysis, 300 µL of the molybdic acid solution was mixed with 3 mL of deionized water and 10 µL of the reaction supernatant (collected immediately after the first centrifugation). The solution began to turn yellow. After exactly 15 minutes, 1.6 mL of the reducing agent solution was added, which initiated the development of a blue colour. The solution was stored at room temperature for 2 to 24 hours, after which the absorbance at 810 nm was recorded using a ThermoFisher spectrophotometer. A standard calibration curve was generated using sodium metasilicate solutions as standards. This analysis was used to quantify the amount of unreacted silicic acid monomer remaining after the reaction.

Separately, the amount of polymeric silica yield was determined by dissolving approximately 5 mg of the final dried product in 2 M NaOH at 80 °C for 1 hour, until the solution became visibly clear. Ten-microliter aliquots were collected, and silicon content was determined as described above. The concentration of silicon in oligomeric form was calculated by subtracting the amount of unreacted monomer and polymeric silica from the initial silicon concentration in the reaction.

## Transmission Electron Microscopy (TEM) and Image Analysis

Transmission Electron Microscopy (TEM) imaging was performed using a JEOL JEM-F200 multipurpose field emission transmission electron microscope operated at an accelerating voltage of 200 kV with a cold field emission gun (FEG) for high brightness and narrow

energy spread during high-resolution TEM (HRTEM) imaging, providing high resolution of synthesised silica nanoparticle populations for nanometrology. Samples from both the MIVM continuous synthesis as well as from the batch reaction were prepared by suspending the materials in isopropanol and depositing them onto standard carbon-coated copper grids. Five images were captured for each sample.

The high-resolution TEM images were analysed using ImageJ.[37] Particle measurements were conducted by manually tracing the particle boundaries using the freehand tool and fitting ellipses over the traced particles. The particle size was calculated as the average of the major and minor axes of the fitted ellipse and the aspect ratio was determined by dividing the length of the minor axis by the length of the major axis. Histograms showing particle size distribution were created from TEM images, with 500 particles analysed for each flow rate.

# Results and discussion

### Validation of the custom-built in-line optical absorption setup

The VD reaction system features a range of unquantified precautions in literature, including light exposure/sensitivity, time-dependant stability and oxygen sensitivity, both for prepared reagents and the products formed after mixing as well as reagent suitability.[24, 33, 34, 38-40] These lead to a lack of reproducibility and user- and lab-biases, and drew our attention to the scatter source in our preliminary manually sampled data despite taking precautions. However, preliminary investigation for a representative VD product in this work showed limited effects from air, light, or time: only a 5% drop in absorbance for a nitrogen degassed/sealed cuvette in the dark over 30 mins, increasing to 7% for an air bubbled cuvette (with or without light) over 30 mins, encouraging further elimination of any variability from manual sampling and improved diagnosis of the experiment. Similarly, other literature has encountered issues with manual VD reaction sampling and recommended on-line monitoring.[41] To this end, an automated custom-built/“DIY” in-line absorbance setup, specifically for VD characterisation, was designed and implemented.

The normal practice is to measure absorbance at 353 nm for quantifying the concentration of the triiodide product. For a DIY apparatus measuring at 353 nm becomes impractical/tedious due to needs of special photosensors, UV LEDs and focussing optics. However, since the triiodide product has appreciable absorption at 405 nm, inexpensive pre-focused LEDs and sensors can be used – these have not been used before. Hence, in order to confirm the validity of the custom-built in-line setup, we performed measurements in two steps: (i) using traditional spectrophotometer, we evaluated whether measuring at 405 nm instead of 353 nm provides a robust strategy. (ii) compared the absorbances at 405 nm between a spectrophotometer and the DIY set-up. The results are discussed below.

Firstly, we used a spectrophotometer to compare the measurements at these two wavelengths (Figure 4a, left Y-axis). Sequential slow addition of the two VD system components provided a range of absorbance values. A direct correlation was observed, with an absorbance ratio of 19.3%, satisfactorily close to the literature value of 19.9%[32] thus showing no evidence of a confounding secondary absorbing species at this alternate wavelength. This confirms that measuring triiodide absorbance at 405 nm still provides accurate results. Next, we compared the absorbance at 405 nm obtained from the DIY setup with the measurements from the spectrophotometer, also at 405 nm (Figure 4a, right Y-axis) with the cuvette tested alternately first in the spectrophotometer then the in-line setup to mitigate solution time sensitivity. We see an excellent agreement between the two measurements from the in-line setup and spectrophotometer, showing linearity up to an absorbance of 0.5. The slope of 0.96553, vs. 1 is negligibly different, likely due to inexact LED wavelength specification, or the LED's slightly broadband output coupled with operating on the side of an absorbance peak. This confirms that the DIY set-up provides excellent accuracy when measuring triiodide.

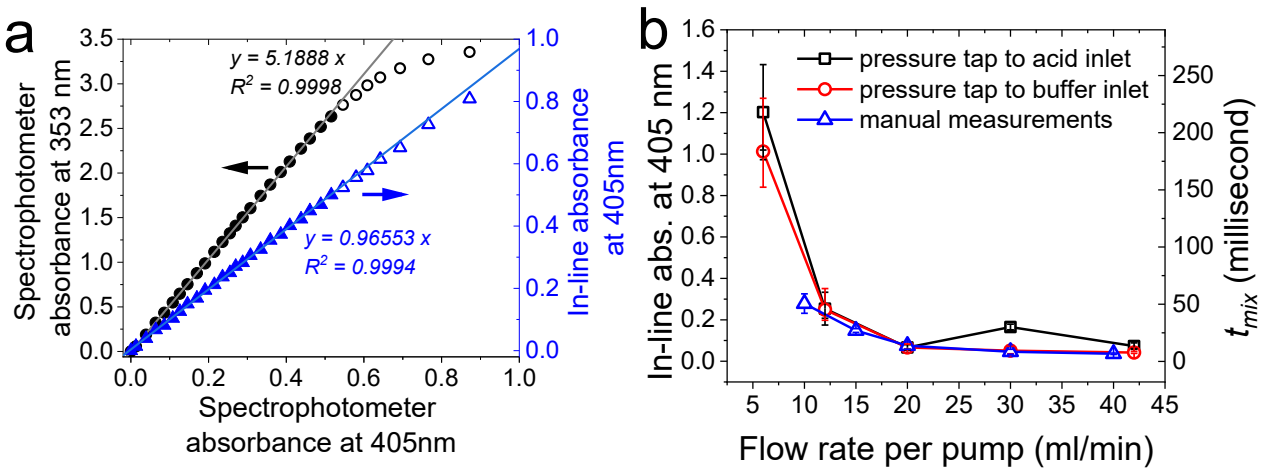


Figure 4: (a) Comparison of UV-VIS spectrophotometer absorbance at 405nm and at 353 nm (left axis, circles) for Villermaux-Dushman products and a comparison of the in-line apparatus with a spectrophotometer, both measuring VD products at 405 nm (right axis, triangles). Solid lines are linear best fits through the solid filled data points, while the hollow data points were as they were outside the linearity region. The linear region helped identify the linear region for designing next experiments. (b) Absorbance and $t_{mix}$ (via lookup) VD results for the MIVM across a range of flowrate conditions for multiple experimental runs, averaged (error bars based on max-min values within one experimental run from time series data, averaged). Experiments were conducted for both orientations of the MIVM ports (black and red). Preliminary manually sampled data is also shown (blue data points), measured at 353 nm and converted to 405 nm via data in (a).

These results open the possibility of using custom-built in-line measurements, which can be readily built. The in-line setup demonstrated excellent ability to monitor VD reaction products whilst providing additional practical insights, and, in turn, can provide a rapid and versatile platform for quantifying mixing.

## Villermaux-Dushman mixing characterisation

After validating the analytics of the in-line setup, next, we use it to characterise the MIVM and associated mixing using VD reactions. The results are plotted in Figure 4b for four repeats at each flowrate with error bars showing the max and min values, for both mixer orientations. The manually sampled VD data is also plotted in Figure 4b (arbitrary mixer orientation) for comparison. For the MIVM with the pressure tap side fed with buffer solution, we see the expected trend with absorbance and thus $t_{mix}$ values decreasing with increasing flowrate. When we reversed the MIVM orientation, swapping the acid and buffer ports, a

similar trend was produced, except at 30 ml/min, a slightly higher absorbance was observed. Nevertheless, the mixing times calculated for these flowrates (~200 ms for 6 ml/min and 10-50 ms for the rest of the flowrates) are comparable to the results reported in the literature using MIVMs of similar geometries.[13, 15] Finally, the results from the in-line measurements were corroborated with those previously obtained from our traditional manual (off-line) measurements. This comparison, shown in Figure 4b, shows excellent match, further confirming the successful use of the DIY setup.

## Bioinspired silica synthesis using MIVM

After characterising the mixer, we used the MIVM for the synthesis of bioinspired silica to investigate its benefits, especially in developing scalable synthesis. In order to assess the performance of the MIVM and the materials produced, we measured the precursor conversion and product yield to assess the efficiency of the process. The materials formed were then characterised for their porosity and particle sizes as measures of the product quality. Figure 5a presents the results from measuring the silicate species concentrations at varying flow rates (6, 12, 20, 30, 42 ml/min/pump) and a small scale batch stirred reaction as a reference, which represents an ideally mixed system. The graph shows the resulting product distribution in three distinct forms: monomeric silica or silicic acid (the precursor) that is not converted, oligomeric silicates (the intermediate) that remains in the supernatant even after centrifugation, and polymeric silica (product) that is collected as solids upon centrifugation (see Equation 4 for the reaction scheme).

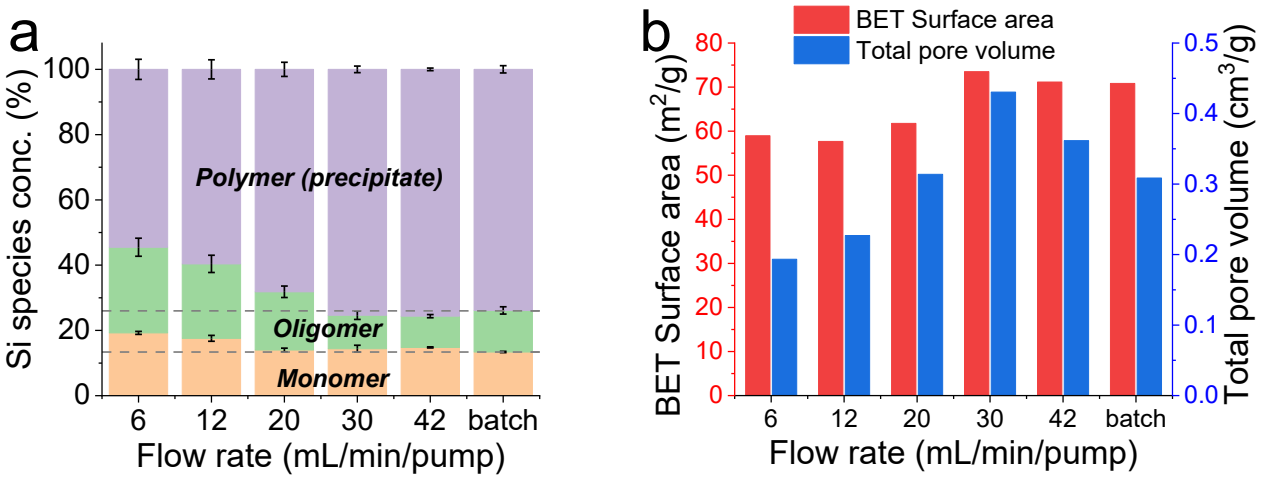


Figure 5: (a) Silicate speciation showing unreacted monomer/precursor, oligomers (that are not precipitated) and final product (precipitated polymeric silica) for reactions conducted under different flow rates and under batch conditions. (b) Surface area and pore volume data for bioinspired silica samples produced at different flow rates in comparison with those produced in a small scale batch.

At lower flow rates (longer mixing times), relatively more silicic acid monomer remains in the solution after the reaction (~18% vs. ~13% for batch), which represents lower conversion. This is coupled with higher oligomer concentration (~25% vs. ~13% for batch) and lower yield of the product (~57% vs. ~74% for batch). As the flow rate increased (>20 ml/min, i.e. faster mixing), a shift in the product distribution was observed such that the conversion of the monomer and the yield of the product approached those seen for the batch reaction, which is consistent to previous work.[6] Poor mixing/longer mixing time (roughly over 10 milliseconds) at lower flowrates caused a heterogeneous reaction environment and oligomers are unable to grow/aggregate further to precipitate and hence a lower yield. As the flow rate increased (mixing times roughly below 10 milliseconds), a more homogenous reaction environment is achieved, leading to a higher yield of polymeric silica.

In Figure 5b, we observe the relationship between mixing time and the porosity (surface area and pore volume) of BIS produced. Similar to the speciation of silicates, surface areas of BIS obtained at higher flowrates and batch synthesis were similar, while those obtained at lower flowrates (slow mixing) were little lower. This is likely due to wider particle size distributions discussed below), which may lead to tighter packing. We note that the surface areas were

generally low compared to typically reported bioinspired silica, due to the amine additives still found occupying the pores.[42]

The materials produced were further imaged using TEM to study the particle sizes (Figure 6a-f) and the particle size distributions (PSD) shown in Figure 6g for each flowrate studied as well as for the batch reaction. At the low flow rate (≤20 ml/min), the average particle sizes were higher (60-80 nm) with broad PSD (full width at half maximum was 35-55 nm). As the flow rate increased (>20 ml/min) causing with faster mixing, the distribution became narrower (full width at half maximum was ~23 nm), with the average particle sizes shifting toward smaller diameters (~40 nm). The results on silicate speciation and product properties confirm the benefits of better mixing being achieved by using MIVM for BIS synthesis. This is consistent with previous work reported on traditional silica synthesis where it was demonstrated that using microreactors or micromixers helps controlling particle size distributions and improving reactant conversions compared to traditional batch reactors.[10]

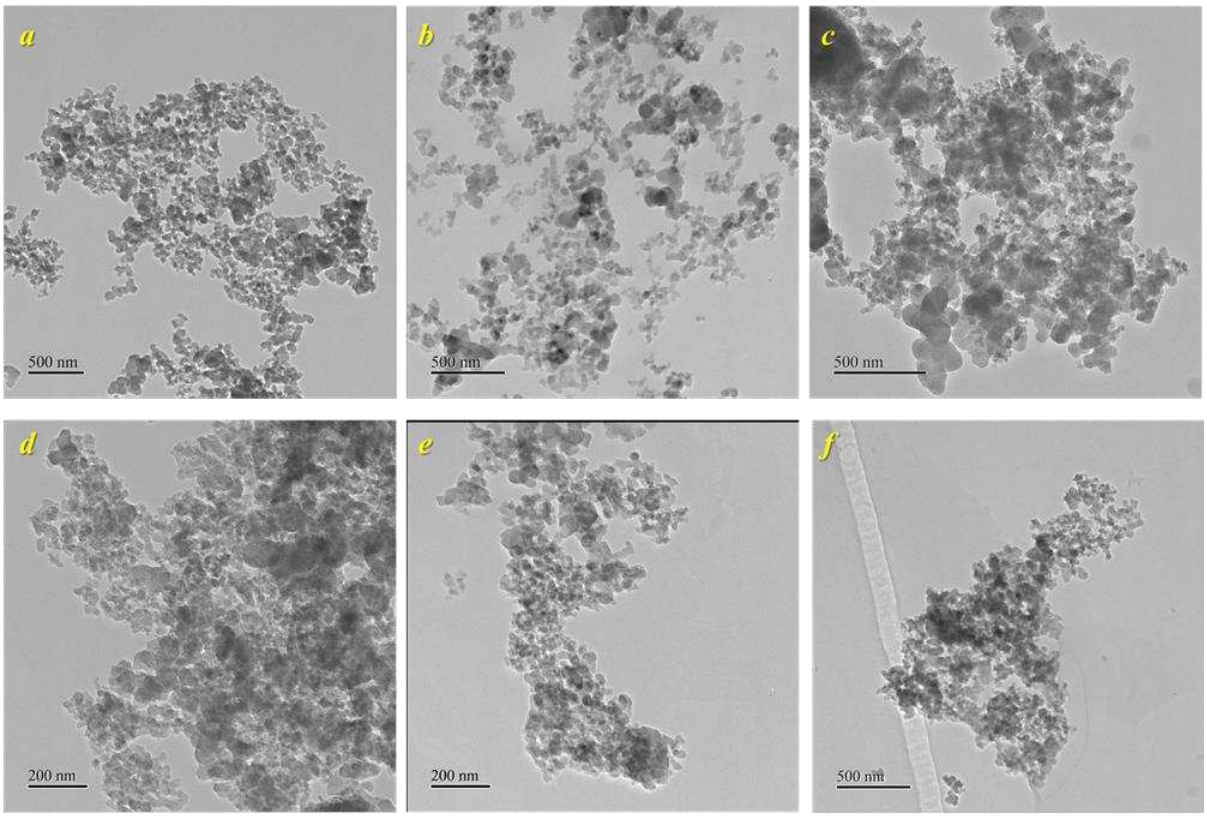

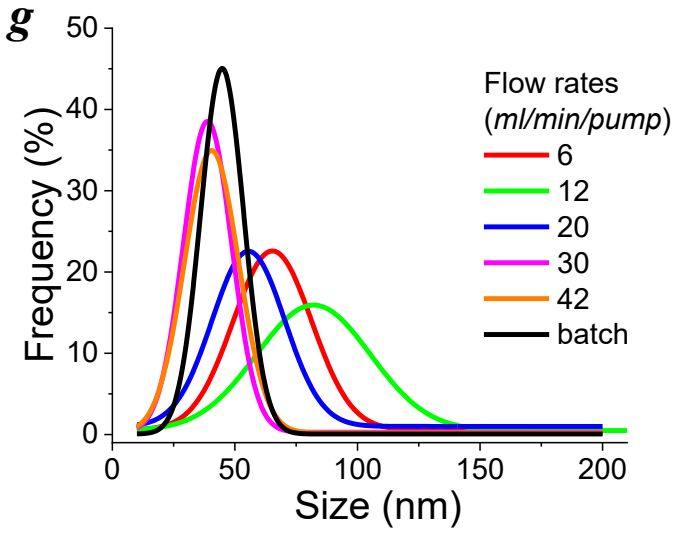


Figure 6: Transmission electron micrographs of bioinspired silica samples produced at different flow rates (a-e: 6, 12, 20, 30 and 42 ml/min respectively) in comparison with those produced in a small scale batch (f). Scale bars: 500 nm for a-c, f and 200 nm for d, e. (g) Particle size distribution for each sample.

# Conclusions

We constructed an in-line setup and demonstrated its facile use in rapid and continuous monitoring of VD reactions, mitigating any issues caused by manual sampling and sampling delays, providing additional diagnostics, while also avoiding a need for high-spec spectrophotometer. The results show that the custom-built in-line setup was successfully able to characterise mixing in MIVM. The MIVM and associated information on its mixing profiles were used for the first time to perform bioinspired silica synthesis and the results confirmed the benefits of MIVM use in studying the impact of mixing on silica particle sizes, porosity and yield. The results identified a consistent trend in particle size distribution, yield and surface area analyses, where a critical flowrate or mixing time (~10 milliseconds) seem to exist. These insights and the ability to reproducibility and rapidly scope in-line mixers with the hardware described herein also forms a platform for rapidly scaling up novel materials synthesis. The results also identified the range of flowrates that produce desired mixing for BIS synthesis, which will help design larger scale manufacturing process and equipment. While our future work is addressing the underpinning mixing mechanisms by undertaking

extensive experimental and computational fluid dynamics research, these results demonstrate that the multi-inlet vortex mixer is a promising tool to unlock the scalability of novel synthesis of nanomaterials.

# Acknowledgements

We thank EPSRC for funding this research (EP/R025983/1 and EP/V051458/1). TEM imaging was conducted at the Sorby Centre for Electron Microscopy. We would also like to thank Luc DeWulf (School of Chemical, Materials and Biological Engineering, The University of Sheffield) for assistance in 3D printing the first prototypes of our in-line absorbance setup in the University of Sheffield *iForge Makerspace*. We thank Professor Daniele Marchisio (Torino) and Professor Vivek Ranade (Limerick) for advice and helpful discussions.

# References

1. S. V. Patwardhan and S. S. Staniland, *Green Nanomaterials: From Bioinspired Synthesis to Sustainable Manufacturing of Inorganic Nanomaterials*, IoP Publishing, 2020.
2. C. Brambila, P. Boyd, A. Keegan, P. Sharma, C. Vetter, E. Ponnusamy and S. V. Patwardhan, *ACS Sustainable Chemistry & Engineering*, 2022, **10**, 5288-5298.
3. C. Drummond, R. McCann and S. V. Patwardhan, *Chemical Engineering Journal*, 2014, **244**, 483-492.
4. S. V. Patwardhan, J. R. H. Manning and M. Chiacchia, *Current Opinion in Green and Sustainable Chemistry*, 2018, **12**, 110-116.
5. R. Pilling and S. V. Patwardhan, *ACS Sustainable Chemistry & Engineering*, 2022, **10**, 12048-12064.
6. Y. D. Baba, M. Chiacchia and S. V. Patwardhan, *ACS Engineering Au*, 2023, **3**, 17-27.
7. J. R. H. Manning, C. Brambila, K. Rishi, G. Beaucage, G.-L. Davies and S. V. Patwardhan, *ACS Sustainable Chemistry & Engineering*, 2024, **12**, 4900-4911.
8. B. K. Johnson and R. K. Prud'homme, 2003, **49**, 2264-2282.
9. E. Schaer, R. Ravetti and E. Plasari, *Chemical Engineering and Processing: Process Intensification*, 2001, **40**, 277-293.
10. L. Gutierrez, L. Gomez, S. Irusta, M. Arruebo and J. Santamaria, *Chemical Engineering Journal*, 2011, **171**, 674-683.
11. W.-S. Kim and J. M. Tarbell, *Chemical Engineering Communications*, 1999, **176**, 89-113.
12. C. Devos, S. Mukherjee, P. Inguva, S. Singh, Y. Wei, S. Mondal, H. Yu, G. Barbastathis, T. Stelzer, R. D. Braatz and A. S. Myerson, DOI: https://doi.org/10.1002/aic.18595, e18595.
13. Y. Liu, C. Cheng, Y. Liu, R. K. Prud'homme and R. O. Fox, *Chemical Engineering Science*, 2008, **63**, 2829-2842.
14. J. Han, Z. Zhu, H. Qian, A. R. Wohl, C. J. Beaman, T. R. Hoye and C. W. Macosko, *Journal of Pharmaceutical Sciences*, 2012, **101**, 4018-4023.
15. C. E. Markwalter and R. K. Prud'homme, *Journal of Pharmaceutical Sciences*, 2018, **107**, 2465-2471.
16. S. F. Chow, C. C. Sun and A. H. L. Chow, *European Journal of Pharmaceutics and Biopharmaceutics*, 2014, **88**, 462-471.

17. J. Feng, C. E. Markwalter, C. Tian, M. Armstrong and R. K. Prud'homme, *Journal of Translational Medicine*, 2019, **17**, 200.
18. N. Di Patrizio, M. Bagnaro, A. Gaunand, J.-F. Hochepied, D. Horbez and P. Pitiot, *Chemical Engineering Journal*, 2016, **283**, 375-387.
19. D. L. Marchisio, F. Omegna, A. A. Barresi and P. Bowen, *Industrial & Engineering Chemistry Research*, 2008, **47**, 7202-7210.
20. D. L. Marchisio, F. Omegna and A. A. Barresi, *Chemical Engineering Journal*, 2009, **146**, 456-465.
21. M. Hussain, R. Ceccarelli, D. L. Marchisio, D. Fino, N. Russo and F. Geobaldo, *Chemical Engineering Journal*, 2010, **157**, 45-51.
22. S. Bensaid, F. A. Deorsola, D. L. Marchisio, N. Russo and D. Fino, *Chemical Engineering Journal*, 2014, **238**, 66-77.
23. M. L. Para, M. Alidoost, M. Shiea, G. Boccardo, A. Buffo, A. A. Barresi and D. Marchisio, *Chemical Engineering Science*, 2022, **254**.
24. J.-M. Commenge and L. Falk, *Chemical Engineering and Processing: Process Intensification*, 2011, **50**, 979-990.
25. T. Frey, F. Kexel, M. Grabellus, X. M. Le, M. Hoffmann, F. Herbstritt, M. Grünewald and M. Schlüter, *Chemical Engineering Research and Design*, 2024, **205**, 822-829.
26. J. M. Reckamp, A. Bindels, S. Duffield, Y. C. Liu, E. Bradford, E. Ricci, F. Susanne and A. Rutter, *Organic Process Research & Development*, 2017, **21**, 816-820.
27. Z. Lan and Y. Lu, *Micromachines* 2023, **14**, 45.
28. Y. Asano, S. Togashi and Y. Endo, *JOURNAL OF CHEMICAL ENGINEERING OF JAPAN*, 2013, **46**, 770-776.
29. M. Kashid, A. Renken and L. Kiwi-Minsker, *Chemical Engineering Journal*, 2011, **167**, 436-443.
30. A. Kölbl and S. Schmidt-Lehr, *Chemical Engineering Science*, 2010, **65**, 1897-1901.
31. J. R. Bourne, *Chemical Engineering Journal*, 2008, **140**, 638-641.
32. S. V. Kireev and S. L. Shnyrev, *Laser Physics*, 2015, **25**, 075602.
33. L. Liu, X. Yang, J. Yang, G. Li and Y. Guo, *AIChE J.* , 2021, **67**, e17225.
34. P. Guichardon and L. Falk, *Chemical Engineering Science*, 2000, **55**, 4233-4243.
35. J. R. H. Manning, E. Routoula and S. V. Patwardhan, *Journal of Visualised Experiments*, 2018, **138** e57730.
36. D. Belton, G. Paine, S. V. Patwardhan and C. C. Perry, *Journal of Materials Chemistry*, 2004, **14**, 2231-2241.
37. C. A. Schneider, W. S. Rasband and K. W. Eliceiri, *Nature Methods*, 2012, **9**, 671-675.
38. S. R. L. Gobert, S. Kuhn, L. Braeken and L. C. J. Thomassen, *Organic Process Research & Development*, 2017, **21**, 531-542.
39. P. Guichardon, L. Falk and J. Villermaux, *Chemical Engineering Science*, 2000, **55**, 4245-4253.
40. C. Baqueiro, N. Ibaseta, P. Guichardon and L. Falk, *Chemical Engineering Research and Design*, 2018, **136**, 25-31.
41. O. S. Okwundu, M. Fuseini, A. H. El-Shazly and M. F. Elkady, *Journal of the Serbian Chemical Society*, 2020, **85**, 381.
42. J. R. H. Manning, T. W. S. Yip, A. Centi, M. Jorge and S. V. Patwardhan, 2017, **10**, 1683-1691.

# Supporting Information

## Rapid, in-line characterisation of a vortex mixer and its use for green synthesis of nanosilica

*Richard Hodgkinson[#], Carlos Brambila[#], John Nutter, Siddharth Patwardhan**

*School of Chemical, Materials and Biological Engineering,*
*The University of Sheffield, Mappin Street, Sheffield, S1 3JD, UK*
*[#] These authors contributed equally.*
** Corresponding author: s.patwardhan@sheffield.ac.uk*

To show and explain critical features of the experiment, Figure S1 plots absorbance data time series from one of the VD characterisation experimental runs using the custom in-line optical setup. Under automatic control, each of the five flowrates was successively run. Dark (shutter closed) - bright (pure water flush) level resets were conducted before 6, 20 and 42ml/min, shown with arrows in Figure S1 as breaks in the data series. Changes in transmission on bright or dark resets was typically less than 1% and scattered in sign, showing the in-line setup electronics to be suitably stable, and surprisingly, that the polystyrene cuvette used appears unaffected by the iodine coating issue.

Each flowrate test consisted of a period of steady pumping and stir bar rotation within the cuvette (section A in Figure S1) for a fixed volume of reagents, stir bar rotation only (section B in Figure S1), and measurement without pumping or stirring (section C in Figure S1). Spikes in absorbance tend to occur at the start of pumping due to regions of high triiodide concentration forming at rest which are subsequently mixed and flushed through.

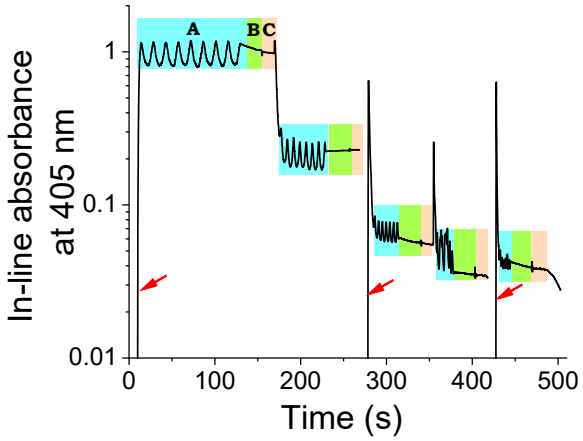


Figure S1: Example Villermaux-Dushman in-line absorbance data time series. Flowrates were run sequentially: 6, 12, 20, 30, and 42ml/min. Light/dark level resets have been omitted for clarity (breaks in the data series, marked by red arrows). Letters show exemplar sections within the 6ml/min run (A: pumping and stirring, B: stirring only, C: no pumping or stirring). The data set shown corresponds to a run with the MIVM pressure tap side fed with buffer solution.

Immediately apparent from Figure S1 is the oscillation in absorbance levels during pumping (section A only). We directly attributed this to variations in flowrate from the syringe pumps, and not from motor stepping as commonly assumed. Since glass syringes minimised the "stick-slip" effects of disposable, rubber tipped syringes and the oscillations occurred once per leadscrew revolution, we suspect flexing of the syringe driving plate's motion. Manual sampling thus extracts samples at random points in this cycle, causing the apparent absorbance variability. Flowrate variations were subsequently confirmed by pressure drop across a restriction (data not shown). This is an important point: these particular make/model of syringe pumps are extremely common in laboratories and while they dose fluids accurately on average, at short timescales, the flow instabilities are likely not appreciated. As a result, here instead of reporting absorbance from section C as originally intended, since minimal time was taken to reach "steady state" in section A and final stirring in section B had minimal impact, we instead extract average, maximum and minimum absorbance values over section A for each flowrate over an integer number of oscillation cycles, and average these values over four repeat experiments.